

# Early cosmic merger of multiple black holes

H. Tagawa,<sup>1,2★</sup> M. Umemura,<sup>3</sup> N. Gouda,<sup>1,2</sup> T. Yano<sup>2</sup> and Y. Yamai<sup>4</sup>

<sup>1</sup>*Department of Astronomy, Graduate school of Science, The University of Tokyo, 7-3-1 Hongo Bunkyo, Tokyo 113-0033, Japan*

<sup>2</sup>*National Astronomical Observatory of Japan, 2-21-1 Osawa, Mitaka, Tokyo 181-8588, Japan*

<sup>3</sup>*Center for Computational Sciences, University of Tsukuba, Tsukuba, Ibaraki 305-8577, Japan*

<sup>4</sup>*Mitsubishi Space Software Co. Ltd.*

Accepted 2015 May 12. Received 2015 May 9; in original form 2015 April 7

## ABSTRACT

We perform numerical simulations on the merger of multiple black holes (BHs) in primordial gas at early cosmic epochs. We consider two cases of BH mass:  $M_{\text{BH}} = 30$  and  $10^4 M_{\odot}$ . Attention is concentrated on the effect of the dynamical friction by gas in a host object. The simulations incorporate such general relativistic effects as the pericentre shift and gravitational wave emission. As a result, we find that multiple BHs are able to merge into one BH within 100 Myr in a wide range of BH density. The merger mechanism is revealed to be categorized into three types: gas-drag-driven merger (type A), interplay-driven merger (type B), and three-body-driven merger (type C). We find the relation between the merger mechanism and the ratio of the gas mass within the initial BH orbit ( $M_{\text{gas}}$ ) to the total BH mass ( $\sum M_{\text{BH}}$ ). Type A merger occurs if  $M_{\text{gas}} \gtrsim 10^5 \sum M_{\text{BH}}$ , type B if  $M_{\text{gas}} \lesssim 10^5 \sum M_{\text{BH}}$ , and type C if  $M_{\text{gas}} \ll 10^5 \sum M_{\text{BH}}$ . Supposing the gas and BH density based on the recent numerical simulations on first stars, all the BH remnants from first stars are likely to merge into one BH in  $\sim 10^7$  yr through the type B or C mechanism. Also, we find that multiple massive BHs ( $M_{\text{BH}} = 10^4 M_{\odot}$ ) distributed over several parsec can merge into one BH through the type B mechanism, if the gas density is higher than  $5 \times 10^6 \text{ cm}^{-3}$ . The present results imply that the BH merger may contribute significantly to the formation of supermassive BHs at high-redshift epochs.

**Key words:** gravitational waves – methods: numerical – galaxies: high-redshift – dark ages, reionization, first stars.

## 1 INTRODUCTION

In the last two decades, it has been demonstrated that massive galaxies harbour supermassive black holes (SMBHs) in the centres of their bulge components (Kormendy & Ho 2013, and references therein). Also, at redshifts higher than 6, quasars are found that possess SMBHs with the mass higher than  $10^9 M_{\odot}$  (Fan et al. 2001; Kurk et al. 2007). The formation history of these SMBHs is among the most significant unsolved issues in astrophysics (Volonteri & Bellovary 2012; Haiman 2013). Two recently discovered high-redshift quasars, ULAS J112010+641 with the mass of  $M_{\text{BH}} = 2 \times 10^9 M_{\odot}$  at redshift  $z = 7.085$  (Mortlock et al. 2011) and SDSS J01001+2802 with  $M_{\text{BH}} = 1.2 \times 10^{10} M_{\odot}$  at  $z = 6.30$  (Wu et al. 2015) have raised a serious problem for the formation of SMBHs. Possible building blocks for such high-redshift SMBHs are the remnants of first stars. The initial mass function of first stars is thought to be more or less top-heavy (Abel, Bryan & Norman 2000; Nakamura & Umemura 2001; Bromm, Coppi & Larson 2002; Yoshida et al. 2006; Greif et al. 2011; Hirano et al. 2014;

Susa, Hasegawa & Tominaga 2014). First stars of several tens  $M_{\odot}$  undergo supernovae, leaving black holes (BHs) of few tens  $M_{\odot}$  (Heger & Woosley 2002). For SMBHs to grow from such first star remnants through mass accretion at  $z \gtrsim 6$ , a super-Eddington accretion rate is requisite. If SMBHs grow continuously by mass accretion from BH remnants of  $\sim 20 M_{\odot}$ , the Eddington ratio ( $\lambda$ ) is required to be  $\lambda = 1.4$  for ULAS J112010+641, or  $\lambda = 1.3$  for SDSS J01001+2802. However, the continuous accretion is unlikely to be sustained due to feedbacks, and thus the average mass accretion rates should be lower than the Eddington rate (Alvarez, Wise & Abel 2009; Milosavljevic, Couch & Bromm 2009). On the other hand, seed BHs may stem from supermassive stars of  $10^{4-6} M_{\odot}$  as a result of the direct collapse of primordial density fluctuations (Umemura, Loeb & Turner 1993; Bromm & Loeb 2003; Inayoshi & Omukai 2012). These BHs are thought to be incorporated into a primordial galaxy of  $\sim 10^8$ – $10^9 M_{\odot}$  (Greene 2012). If an SMBH grows via gas accretion from such a massive BH (MBH), the constraint on the accretion rate can be alleviated.

Another possible pathway of SMBH formation is the merger of BHs. If the merger of multiple BHs precedes the growth via gas accretion, the merged BH can be a seed of a SMBH. So far, the merger of SMBHs in a galaxy has been argued extensively. As for

\* E-mail: tagawahr@nao.ac.jp

a binary of SMBHs, Begelman, Blandford & Rees (1980) pointed out that the orbit of a binary SMBH cannot shrink below 1 pc due to the loss cone depletion (the depletion of stars on orbits that intersect the binary SMBH), which is often called the final parsec problem (e.g. Merritt & Poon 2004). It is argued that if the host galaxy provides an aspherical potential, a binary SMBH may overcome the final parsec problem (Khan, Just & Merritt 2011; Khan et al. 2012, 2013). However, this solution of the problem is still under debate (Vasiliev, Antonini & Merritt 2014). If there are more than two SMBHs in a galaxy, the dynamical relaxation of SMBHs is significantly controlled by the gravity of SMBHs themselves, especially by three-body interaction. When a third MBH intrudes into a binary SMBH, one SMBH carries away angular momentum from the remaining two SMBHs, reducing the binary separation and eventually inducing the merger of the binary (Iwasawa, Funato & Makino 2006). In the case of many SMBHs, the stellar dynamical friction allows a binary MBH to interact frequently with other SMBHs, and then the decay of the binary orbits leads to the merger (Tanikawa & Umemura 2011, 2014).

In a first-generation object formed at an early cosmic epoch, the dynamical friction by stars is unlikely to work effectively, since the initial mass function is top-heavy and most stars undergo supernovae. However, the dynamical friction by gas could work. Recent radiation hydrodynamic simulations on the formation of first stars show that several or more stars form in a primordial gas cloud with the density of around  $10^7 \text{ cm}^{-3}$  and the extension of 1000 au, where the gas fraction is 99 percent (Greif et al. 2011; Umemura et al. 2012; Susa 2013; Susa et al. 2014). In this circumstance, BH remnants of first stars are most likely subject to the dynamical friction by abundant gas. The gas dynamical friction has been considered as a mechanism that prompts the BH merger (Ostriker 1999; Tanaka & Haiman 2009). Hitherto, the merger processes by the gas dynamical friction have been investigated in the case of two MBHs (e.g. Escala et al. 2004, 2005). In this paper, we explore the merger of multiple BHs, supposing a first-generation object of  $\sim 10^5\text{--}10^6 M_\odot$  or a gas-rich primordial galaxy of  $\sim 10^8\text{--}10^9 M_\odot$ .

The paper is organized as follows. In Section 2, we describe the numerical method. In Section 3, we show the numerical results. In Section 4, we discuss the merger criterion through the gas friction. In Section 5, we summarize the paper.

## 2 METHOD OF NUMERICAL SIMULATIONS

Here, we present the framework of numerical simulations.

### 2.1 Equation of motion

The equations of motion for BHs are given by

$$\frac{d^2 \mathbf{r}_i}{dt^2} = \sum_j^{N_{\text{BH}}} \left\{ -Gm_j \frac{\mathbf{r}_i - \mathbf{r}_j}{|\mathbf{r}_i - \mathbf{r}_j|^3} + \mathbf{a}_{\text{PN},ij} \right\} + \mathbf{a}_{\text{DF},i}^{\text{gas}} + \mathbf{a}_{\text{pot},i}, \quad (1)$$

where  $\mathbf{r}_i$  and  $\mathbf{r}_j$  are, respectively, the positions of  $i$ th BH and  $j$ th BH,  $N_{\text{BH}}$  is the number of BHs,  $G$  is the gravitational constant,  $m_j$  is the mass of  $j$ th BH,  $\mathbf{a}_{\text{PN},ij}$  is the general relativistic acceleration of  $j$ th BH on  $i$ th BH in the post-Newtonian prescription,  $\mathbf{a}_{\text{DF},i}^{\text{gas}}$  is the dynamical friction (DF) on  $i$ th BH by gas, and  $\mathbf{a}_{\text{pot},i}$  is the acceleration on  $i$ th BH by gravitational potential of gas.

### 2.2 Key parameters

We initially set up multiple BHs of equal mass. In this paper, we consider two cases of the BH mass: one is  $30 M_\odot$  BHs as first star remnants, which are born in a first-generation object of  $\sim 10^5\text{--}10^6 M_\odot$ , and the other is  $10^4 M_\odot$  BHs resulting from supermassive stars, which are incorporated into a primordial galaxy of  $\sim 10^8\text{--}10^9 M_\odot$ . A key parameter in the present simulations is the BH density,  $\rho_{\text{BH}}$ , at the initial epoch. Recent radiation hydrodynamic simulations on first star formation have shown that several or more stars are born in a disc of  $\sim 1000$  au (Greif et al. 2011; Umemura et al. 2012; Susa 2013; Susa et al. 2014). We change the typical extension of the BH distribution at the initial epoch,  $r_{\text{typ}}$ , to settle the BH density. In the case of  $30 M_\odot$  mass BH, we alter  $r_{\text{typ}}$  from 0.01 to 1 pc. In the case of  $10^4 M_\odot$  mass BH, we set  $r_{\text{typ}}$  from 0.1 to 10 pc. Then, the BH density is given by

$$\rho_{\text{BH}} = \frac{3}{4\pi r_{\text{typ}}^3} \sum_i m_i, \quad (2)$$

where  $m_i$  is the mass of  $i$ th BH. Another key parameter is the gas number density  $n_{\text{gas}}$ . Simulations of first stars show that the density in a first object is  $\sim 10^{7\text{--}8} \text{ cm}^{-3}$  in the star formation epoch. Here, we consider a wider range of the gas density from  $10^4$  to  $10^{12} \text{ cm}^{-3}$  to elucidate the dependence of the BH merger on the gas density.

### 2.3 Gas drag and potential

We give the gas dynamical friction and the gas potential by analytic solutions. We use the formula of the gas dynamical friction force given by Tanaka & Haiman (2009) for the motion with  $\mathcal{M}_i < \mathcal{M}_{\text{eq}}$  and Ostriker (1999) for  $\mathcal{M}_i > \mathcal{M}_{\text{eq}}$ , where  $\mathcal{M}_i$  is the Mach number of  $i$ th BH and  $\mathcal{M}_{\text{eq}}$  is the Mach number where these two formulas give equal acceleration. Here, we adopt  $\mathcal{M}_{\text{eq}} = 1.5$  as Tanaka & Haiman (2009). Then, the acceleration of the gas dynamical friction ( $\mathbf{a}_{\text{DF},i}^{\text{gas}}$ ) is given by

$$\mathbf{a}_{\text{DF},i}^{\text{gas}} = -4\pi G^2 m_i m_{\text{H}} n_{\text{gas}}(r) \frac{\mathbf{v}_i}{v_i^3} f(\mathcal{M}_i), \quad (3)$$

$$f(\mathcal{M}_i) = \begin{cases} 0.5 \ln \left( \frac{v_i t}{r_{\text{min}}} \right) \left[ \text{erf} \left( \frac{\mathcal{M}_i}{\sqrt{2}} \right) - \sqrt{\frac{2}{\pi}} \mathcal{M}_i \exp \left( -\frac{\mathcal{M}_i^2}{2} \right) \right], & (0 \leq \mathcal{M}_i \leq 0.8), \\ 1.5 \ln \left( \frac{v_i t}{r_{\text{min}}} \right) \left[ \text{erf} \left( \frac{\mathcal{M}_i}{\sqrt{2}} \right) - \sqrt{\frac{2}{\pi}} \mathcal{M}_i \exp \left( -\frac{\mathcal{M}_i^2}{2} \right) \right], & (0.8 \leq \mathcal{M}_i \leq \mathcal{M}_{\text{eq}}), \\ \frac{1}{2} \ln \left( 1 - \frac{1}{\mathcal{M}_i^2} \right) + \ln \left( \frac{v_i t}{r_{\text{min}}} \right), & (\mathcal{M}_{\text{eq}} \leq \mathcal{M}_i), \end{cases} \quad (4)$$

where  $m_{\text{H}}$  is the mass of the hydrogen atom,  $n_{\text{gas}}$  is the number density of gas,  $v_i$  is the velocity of  $i$ th BH, and  $t$  is the elapsed time. The  $r_{\text{min}}$  is the minimum scale of the dynamical friction on a BH, and we give  $r_{\text{min}}$  as  $Gm_i/v_i^2$ . Here,  $v_i t$  means the effective scale of gas medium, and we set an upper limit of  $v_i t$  to 0.1 pc. When  $v_i t < r_{\text{min}}$ , we assume  $f(\mathcal{M}_i) = 0$ .

In this paper, we postulate uniform background gas to purely extract the dependence on the gas density, and give its density as

a parameter. Then, the gravitational acceleration by gas ( $\mathbf{a}_{\text{pot},i}$ ) and its time derivative ( $\dot{\mathbf{a}}_{\text{pot},i}$ ) are given as

$$\mathbf{a}_{\text{pot},i} = -\frac{4}{3}\pi G m_{\text{H}} n_{\text{gas}} \mathbf{r}_i, \quad (5)$$

$$\dot{\mathbf{a}}_{\text{pot},i} = -\frac{4}{3}\pi G m_{\text{H}} n_{\text{gas}} \mathbf{v}_i. \quad (6)$$

## 2.4 Gas temperature

The heating rate due to the gas dynamical friction is estimated as follows (Kim, El-Zant & Kamionkowski 2005):

$$\begin{aligned} \Lambda_{\text{DF}} &= 7.3 \times 10^{-25} \text{ erg cm}^{-3} \text{ s}^{-1} \left( \frac{n_{\text{gas}}}{10^4 \text{ cm}^{-3}} \right) \\ &\times \left( \frac{M_{\text{BH}}}{30 M_{\odot}} \right)^2 \left( \frac{\langle f(\mathcal{M})/\mathcal{M} \rangle}{2} \right) \\ &\times \left( \frac{T}{1000 \text{ K}} \right)^{-1/2} \left( \frac{n_{\text{BH}}}{10 \text{ pc}^{-3}} \right), \end{aligned} \quad (7)$$

where  $n_{\text{BH}}$  is the number density of BHs, and the angular brackets denote the average over the Maxwellian distribution:

$$f(v) = \frac{4\pi N_{\text{BH}}}{(2\pi\sigma_r^2)^{3/2}} v^2 e^{-v^2/(2\sigma_r^2)}, \quad (8)$$

where  $\sigma_r$  is the one-dimensional velocity dispersion.

In a first object, the cooling is dominated by hydrogen molecules ( $\text{H}_2$ ) at  $T \approx 10^3$  K (e.g. Omukai 2000). In a primordial galaxy, the temperature goes down by the cooling of neutral hydrogen ( $\text{H I}$ ) around  $T \approx 10^4$  K, and further reduces by the  $\text{H}_2$  cooling down to  $T \approx 10^3$  K, if the gaseous metallicity is lower than a per cent of solar abundance (Susa & Umemura 2004). The  $\text{H}_2$  cooling rate through  $\text{H}-\text{H}_2$  collision (Hollenbach & McKee 1989) and the  $\text{H I}$  cooling rate (Thoul & Weinberg 1995) are, respectively, given by

$$\begin{aligned} \Lambda_{\text{H}_2} (10^3 \text{ K}) &= 2.8 \times 10^{-21} \text{ erg cm}^{-3} \text{ s}^{-1} \\ &\times \left( \frac{n_{\text{gas}}}{10^4 \text{ cm}^{-3}} \right) \left( \frac{f_{\text{H}_2}}{3 \times 10^{-4}} \right), \end{aligned} \quad (9)$$

$$\begin{aligned} \Lambda_{\text{H I}} (10^4 \text{ K}) &\sim 1.0 \times 10^{-14} \text{ erg cm}^{-3} \text{ s}^{-1} \\ &\times \left( \frac{n_{\text{gas}}}{10^4 \text{ cm}^{-3}} \right)^2 f_{\text{H I}}^2, \end{aligned} \quad (10)$$

where  $f_{\text{H}_2}$  is the fraction of  $\text{H}_2$  molecules and  $f_{\text{H I}}$  is the fraction of neutral hydrogen atoms. Here,  $f_{\text{H}_2} \gtrsim 3 \times 10^{-4}$  in the range of  $n_{\text{gas}} \gtrsim 10^4 \text{ cm}^{-3}$  (Palla, Salpeter & Stahler 1983).

We find that, in both cases of BH mass, the heating rate is lower than the cooling rate over the range of parameters in which the simulations are performed. Therefore, the gas temperature is expected to settle at  $T \approx 10^3$  K. In this paper, we assume the gas temperature to be 1000 K. Then, the sound speed is given as  $C_s = 3.709 \text{ (km s)}^{-1}$ .

## 2.5 Relativistic effects

We incorporate the general relativistic effects according to the post-Newtonian prescription up to 2.5PN term (Kupi, Amaro-Seoane & Spurzem 2006). The relativistic effects on  $i$ th BH by  $j$ th BH are given by 1PN ( $\mathbf{a}_{1\text{PN},ij}$ ) and 2PN ( $\mathbf{a}_{2\text{PN},ij}$ ) term corresponding to the pericentre shift, and 2.5PN term ( $\mathbf{a}_{2.5\text{PN},ij}$ ) corresponding to the

gravitational wave (GW) radiation. They are expressed by

$$\begin{aligned} \mathbf{a}_{1\text{PN},ij} &= \frac{Gm_j}{r_{ij}^2} \left[ \mathbf{n} \left[ -v_i^2 - 2v_j^2 + 4\mathbf{v}_i \mathbf{v}_j + \frac{3}{2}(\mathbf{nv}_j)^2 \right. \right. \\ &\quad \left. \left. + 5 \left( \frac{Gm_i}{r_{ij}} \right) + 4 \left( \frac{Gm_j}{r_{ij}} \right) \right] \right. \\ &\quad \left. + (\mathbf{v}_i - \mathbf{v}_j)(4\mathbf{nv}_i - 3\mathbf{nv}_j) \right], \end{aligned} \quad (11)$$

$$\begin{aligned} \mathbf{a}_{2\text{PN},ij} &= \frac{Gm_j}{r_{ij}^2} \left[ \mathbf{n} \left[ -2v_j^4 + 4v_j^2(\mathbf{v}_i \mathbf{v}_j) - (\mathbf{v}_i \mathbf{v}_j)^2 \right. \right. \\ &\quad \left. \left. + \frac{3}{2}v_i^2(\mathbf{nv}_j)^2 + \frac{9}{2}v_j^2(\mathbf{nv}_j)^2 - 6(\mathbf{v}_i \mathbf{v}_j)(\mathbf{nv}_j)^2 \right. \right. \\ &\quad \left. \left. - \frac{15}{8}(\mathbf{nv}_j)^4 + \left( \frac{Gm_i}{r_{ij}} \right) \left[ -\frac{15}{4}v_i^2 + \frac{5}{4}v_j^2 \right. \right. \right. \\ &\quad \left. \left. \left. - \frac{5}{2}\mathbf{v}_i \mathbf{v}_j + \frac{39}{2}(\mathbf{nv}_i)^2 - 39(\mathbf{nv}_i)(\mathbf{nv}_j) + \frac{17}{2}(\mathbf{nv}_i)^2 \right] \right. \right. \\ &\quad \left. \left. + \left( \frac{Gm_j}{r_{ij}} \right) \left[ 4v_j^2 + 8\mathbf{v}_i \mathbf{v}_j + 2(\mathbf{nv}_i)^2 \right. \right. \right. \\ &\quad \left. \left. \left. - 4(\mathbf{nv}_i)(\mathbf{nv}_j) - 6(\mathbf{nv}_i)^2 \right] + (\mathbf{v}_i - \mathbf{v}_j) \left[ v_i^2(\mathbf{nv}_j) \right. \right. \right. \\ &\quad \left. \left. \left. + 4v_j^2(\mathbf{nv}_i) - 5v_j^2(\mathbf{nv}_2) - 4(\mathbf{v}_i \mathbf{v}_j)(\mathbf{nv}_i) \right. \right. \right. \\ &\quad \left. \left. \left. + 4(\mathbf{v}_i \mathbf{v}_j)(\mathbf{nv}_j) - 6(\mathbf{nv}_i)(\mathbf{nv}_j)^2 + \frac{9}{2}(\mathbf{nv}_j)^3 \right] \right. \right. \\ &\quad \left. \left. + \left( \frac{Gm_i}{r_{ij}} \right) \left( -\frac{63}{4}\mathbf{nv}_i + \frac{55}{4}\mathbf{nv}_j \right) \right. \right. \\ &\quad \left. \left. + \left( \frac{Gm_j}{r_{ij}} \right) (-2\mathbf{nv}_i - 2\mathbf{nv}_j) \right] \right] \\ &\quad + \frac{G^3 m_j}{r_{ij}^4} \mathbf{n} \left[ -\frac{57}{4}m_i^2 - 9m_j^2 - \frac{69}{2}m_i m_j \right], \end{aligned} \quad (12)$$

$$\begin{aligned} \mathbf{a}_{2.5\text{PN},ij} &= \frac{4}{5} \frac{G^2 m_i m_j}{r_{ij}^3} \left[ (\mathbf{v}_i - \mathbf{v}_j) \left[ -(\mathbf{v}_i - \mathbf{v}_j)^2 \right. \right. \\ &\quad \left. \left. + 2 \left( \frac{Gm_i}{r_{ij}} \right) - 8 \left( \frac{Gm_j}{r_{ij}} \right) \right] + \mathbf{n}(\mathbf{nv}_i - \mathbf{nv}_2) \right. \\ &\quad \left. \left[ 3(\mathbf{v}_i - \mathbf{v}_j)^2 - 6 \left( \frac{Gm_i}{r_{ij}} \right) + \frac{52}{3} \left( \frac{Gm_j}{r_{ij}} \right) \right] \right], \end{aligned} \quad (13)$$

where

$$\mathbf{n} = \frac{\mathbf{r}_{ij}}{r_{ij}}, \quad (14)$$

$$\mathbf{r}_{ij} = (\mathbf{r}_i - \mathbf{r}_j). \quad (15)$$

## 2.6 Merger condition

We assume that two MBHs merge, when their separation is less than 100 times the sum of their Schwarzschild radii:

$$|\mathbf{r}_i - \mathbf{r}_j| < 100 (r_{\text{sch},i} + r_{\text{sch},j}), \quad (16)$$

where  $r_{\text{sch},i}$  is the Schwarzschild radius of  $i$ th BH given by  $2Gm_i/c^2$  with the speed of light  $c$ . At the final stage of merger, the binding energy of a binary BH is transformed to the energy of GW, retaining the mass of each BH. Hence, the BH mass after the merger is just the sum of two MBHs.

## 2.7 Numerical scheme

We integrate the equations of motion using the fourth-order Hermite scheme with the shared time step (Makino & Aarseth 1992). To use the Hermite scheme, we calculate the time derivative of the acceleration by the Newtonian gravity, the gas gravitational potential, and the relativistic force. On the other hand, we treat the dynamical friction of gas to quadratic order, since the formula of the dynamical friction is not as accurate as that of gravity and also the fourth-order scheme is especially requisite during the gravitational three-body interaction between a close BH binary and an intruding BH. Therefore, the time derivative of the gas dynamical friction is not included. Then, the shared time step in the Hermite scheme is given by

$$\Delta t = \min_i \sqrt{\eta \frac{|\mathbf{a}_{\text{Her},i}| |\mathbf{a}_{\text{Her},i}^{(2)}| + |\mathbf{a}_{\text{Her},i}^{(1)}|^2}{|\mathbf{a}_{\text{Her},i}^{(1)}| |\mathbf{a}_{\text{Her},i}^{(3)}| + |\mathbf{a}_{\text{Her},i}^{(2)}|^2}}, \quad (17)$$

where  $\mathbf{a}_{\text{Her},i}$  is the acceleration on  $i$ th BH that is treated to the fourth-order, and given by

$$\mathbf{a}_{\text{Her},i} = \sum_j^{N_{\text{BH}}} \left\{ -Gm_j \frac{\mathbf{r}_i - \mathbf{r}_j}{|\mathbf{r}_j - \mathbf{r}_i|^3} + \mathbf{a}_{\text{PN},ij} \right\} + \mathbf{a}_{\text{pot},i}. \quad (18)$$

The  $\mathbf{a}_{\text{Her},i}^{(k)}$  is the  $k$ th derivative of  $\mathbf{a}_{\text{Her},i}$ , and  $\eta$  is the accuracy parameter. We assume  $\eta = 0.003$  in the present simulations.

To avoid cancellation of significant digits when such tiny scales as  $100 r_{\text{sch}}$  are resolved, we calculate the BHs evolution in the coordinate where the origin is always set to the centre of mass for the closest pair of BHs. This prescription is based on the simulations on the merger of multiple BHs (Tanikawa & Umemura 2011), and allows us to pursue accurately the orbit of the BHs until the merger condition is satisfied.

## 2.8 Set-up of simulations

We set up 10 BHs as a fiducial case, and besides investigate the cases of two or three BHs to scrutinize the key physics of merger. The initial positions of BHs are given randomly in the  $x$ - $y$  plane within  $r_{\text{typ}}$ . Also, we give the velocity to each BH as the sum of a circular component and a random component. The circular velocity is given to balance against the gravity in the  $x$ - $y$  plane. The random velocity is given according to a Gaussian distribution with the same dispersion as the circular velocity. The random velocity is given in the  $xyz$  space. In the case of two BHs, we give only circular velocity without initial eccentricity. This condition is desired to discriminate the BH merger purely by the gas friction.

We calculate each run until 100 Myr, since the background environments of the host objects are likely to change in 100 Myr. Also, we terminate the simulation, if all BHs merge into one BH.

## 3 NUMERICAL RESULTS

### 3.1 Dependence on gas density and BH density

The results of 10 BH systems are summarized in Tables 1 and 2. Table 1 is those for the case of  $M_{\text{BH}} = 30 M_{\odot}$  and Table 2 is for  $M_{\text{BH}} = 10^4 M_{\odot}$ . The column is the initial extension of the BH distribution ( $r_{\text{typ}}$ ) and the corresponding BH density ( $\rho_{\text{BH}}$ ), while the row is the assumed gas density ( $n_{\text{gas}}$ ) in the system.  $N_{\text{m}}$  is the number of the merged BHs (nine means all BHs merged into one). The ‘type’ shows the merger mechanism, which is classified in the next section. Also, the termination time of simulations,  $t_{\text{fin}}$ , is shown.

In the case of  $M_{\text{BH}} = 30 M_{\odot}$  (Table 1), we find that if  $n_{\text{gas}}$  is in the range from  $5 \times 10^6$  to  $10^8 \text{ cm}^{-3}$ , then all the BHs merge into one MBH over six orders of BH density ( $\rho_{\text{BH}} = 72\text{--}7.2 \times 10^7 M_{\odot} \text{ pc}^{-3}$ ). Also, if the gas density is higher than  $n_{\text{gas}} = 5 \times 10^5 \text{ cm}^{-3}$ , the BH merger occurs once at least in 100 Myr. In the recent numerical simulations on first stars (Greif et al. 2011; Susa 2013; Susa et al. 2014), the density of BH remnants is expected to be  $\rho_{\text{BH}} \approx 10^7 M_{\odot} \text{ pc}^{-3}$  and the gas density is to be in the range of  $n_{\text{gas}} \approx 10^7\text{--}10^8 \text{ cm}^{-3}$ . Hence, the present numerical results imply that all the BH remnants from first stars are likely to merge into one BH.

In the case of  $M_{\text{BH}} = 10^4 M_{\odot}$  (Table 2), we find that if  $n_{\text{gas}}$  is in the range from  $5 \times 10^6$  to  $10^9 \text{ cm}^{-3}$ , then all the BHs merge into one MBH over five orders of BH density ( $\rho_{\text{BH}} = 2.4 \times 10^2\text{--}2.4 \times 10^7 M_{\odot} \text{ pc}^{-3}$ ). Interestingly, in the gas denser than  $5 \times 10^6 \text{ cm}^{-3}$ , multiple BHs can merge into one, even if the typical separation is greater than several pc. This result implies that the BH merger is able to contribute significantly to the formation of SMBHs at high redshifts. Similar to the case of  $M_{\text{BH}} = 30 M_{\odot}$ , if the gas density is higher than  $n_{\text{gas}} = 5 \times 10^5 \text{ cm}^{-3}$ , the BH merger occurs once at least.

In both cases of BH mass, if the gas density is very high and simultaneously the BH density is very low (upper left in Tables 1 and 2), no merger occurs. This is due to the fact that the deep gravitational potential by gas enhances the circular velocities of BHs and therefore a self-gravitating system of BHs is hardly able to form.

As shown in terms of the types of merger in Tables 1 and 2, the merger mechanism changes systematically with the gas density ( $n_{\text{gas}}$ ) and the BH density ( $\rho_{\text{BH}}$ ). Details of the merger mechanism are described in the following.

### 3.2 Types of merger mechanism

Here, we scrutinize the merger mechanism and classify the mechanism. When a BH binary merges due to the dynamical friction by gas, the separation of the same pair of BHs monotonically shrinks, while the three-body interaction between a close BH binary and an intruding BH often replaces one BH in the binary by the intruder and therefore the separation of the closest pair changes violently. In Figs 1–5, we show the separation of the closest pair within all BHs as a function of time, where the colours of lines change at every event of the BH merger.

Fig. 1 shows the case of low-mass BHs ( $M_{\text{BH}} = 30 M_{\odot}$ ). The initial extension of the BH distribution is  $r_{\text{typ}} = 1.0 \text{ pc}$ . The upper panel corresponds to higher gas density, and the lower panel to lower gas density. As seen in the upper panel, the apocentre and pericentre distances of the closest pair decay smoothly, eventually resulting in the merger. Such smooth decay indicates that the gas dynamical friction drives the merger. On the hand, in the lower

**Table 1.** The results with  $M_{\text{BH}} = 30 M_{\odot}$  and  $N_{\text{BH}} = 10$ .

$r_{\text{typ}}$ (pc)	1.0		0.464		0.215		0.1		0.0464		0.0215		0.01	
$\rho_{\text{BH}} (M_{\odot} \text{ pc}^{-3})$	$N_{\text{m}}$	Type												
$n_{\text{gas}} (\text{cm}^{-3})$	$t_{\text{fin}}$ (yr)													
$10^{12}$	0	–	5	A	9	A	9	A	9	A	9	A	9	B
	$1.0 \times 10^8$		$1.0 \times 10^8$		$3.6 \times 10^7$		$4.4 \times 10^6$		$1.7 \times 10^6$		$7.0 \times 10^5$		$4.3 \times 10^5$	
$10^{11}$	2	A	8	A	9	A	9	A	9	A	9	A	9	B
	$1.0 \times 10^8$		$1.0 \times 10^8$		$1.3 \times 10^7$		$1.8 \times 10^5$		$1.8 \times 10^5$		$2.3 \times 10^4$		$2.8 \times 10^4$	
$10^{10}$	5	A	9	A	9	A	9	A	9	A	9	B	9	B
	$1.0 \times 10^8$		$4.5 \times 10^7$		$5.1 \times 10^6$		$5.9 \times 10^5$		$7.4 \times 10^4$		$6.3 \times 10^4$		$1.7 \times 10^5$	
$5 \times 10^9$	5	A	9	A	9	A	9	A	9	B	9	B	9	B
	$1.0 \times 10^8$		$2.9 \times 10^7$		$3.1 \times 10^6$		$4.5 \times 10^5$		$1.6 \times 10^5$		$3.4 \times 10^5$		$7.7 \times 10^4$	
$10^9$	8	A	9	A	9	A	9	B	9	B	9	B	9	B
	$1.0 \times 10^8$		$2.4 \times 10^7$		$3.5 \times 10^6$		$2.6 \times 10^5$		$4.3 \times 10^5$		$3.5 \times 10^5$		$3.0 \times 10^5$	
$5 \times 10^8$	8	A	9	A	9	A	9	B	9	B	9	B	9	B
	$1.0 \times 10^8$		$1.2 \times 10^7$		$1.3 \times 10^6$		$6.5 \times 10^5$		$4.3 \times 10^5$		$5.5 \times 10^5$		$5.1 \times 10^5$	
$10^8$	9	A	9	A	9	B	9	B	9	B	9	B	9	B
	$3.0 \times 10^7$		$5.1 \times 10^6$		$4.0 \times 10^6$		$5.5 \times 10^6$		$3.6 \times 10^6$		$4.2 \times 10^6$		$1.2 \times 10^7$	
$5 \times 10^7$	9	A	9	B	9	B	9	B	9	B	9	B	9	B
	$4.5 \times 10^7$		$3.7 \times 10^6$		$2.2 \times 10^7$		$3.2 \times 10^7$		$1.3 \times 10^7$		$4.7 \times 10^6$		$3.6 \times 10^6$	
$10^7$	9	B	9	B	9	B	9	B	9	B	9	B	9	B
	$3.8 \times 10^7$		$2.3 \times 10^7$		$1.7 \times 10^7$		$3.3 \times 10^7$		$1.8 \times 10^7$		$2.9 \times 10^7$		$1.7 \times 10^7$	
$5 \times 10^6$	9	B	9	B	9	B	9	B	9	B	9	B	9	B
	$4.2 \times 10^7$		$3.9 \times 10^7$		$4.2 \times 10^7$		$4.7 \times 10^7$		$6.3 \times 10^7$		$3.5 \times 10^7$		$3.1 \times 10^7$	
$10^6$	6	B	6	B	8	B	6	C	8	C	6	C	6	C
	$1.0 \times 10^8$		$1.0 \times 10^8$		$1.0 \times 10^8$		$1.0 \times 10^8$		$1.0 \times 10^8$		$1.0 \times 10^8$		$1.0 \times 10^8$	
$5 \times 10^5$	2	C	6	C	6	C	4	C	5	C	3	C	4	C
	$1.0 \times 10^8$		$1.0 \times 10^8$		$1.0 \times 10^8$		$1.0 \times 10^8$		$1.0 \times 10^8$		$1.0 \times 10^8$		$1.0 \times 10^8$	
$10^5$	0	–	0	–	1	C	0	–	1	C	2	C	0	–
	$1.0 \times 10^8$		$1.0 \times 10^8$		$1.0 \times 10^8$		$1.0 \times 10^8$		$1.0 \times 10^8$		$1.0 \times 10^8$		$1.0 \times 10^8$	
$10^4$	0	–	0	–	0	–	1	C	0	–	0	–	0	–
	$1.0 \times 10^8$		$1.0 \times 10^8$		$1.0 \times 10^8$		$1.0 \times 10^8$		$1.0 \times 10^8$		$1.0 \times 10^8$		$1.0 \times 10^8$	

panel of Fig. 1, the orbit is highly eccentric, since the apocentre and pericentre distances are largely different. The distances sometimes oscillate violently. Such strong variance is thought to be caused by the three-body interaction, since the simultaneous interaction with a fourth or fifth BH seems quite rare from a viewpoint of probability. Actually, we have confirmed that the contribution of a fourth or fifth BH is little. Thus, we call such interaction the three-body interaction. After the apocentre decays to less than  $\sim 10^{-8}$  pc, the pair separation lessens rapidly due to the effect of the GW emission, and eventually the BH binary merges.

We classify the merger mechanism according to the manner of decay just before the GW promotes the merger. Here, the merger mechanism is categorized into three types: gas-drag-driven merger (type A), three-body-driven merger (type C), and interplay-driven merger (type B). In type A, the dynamical friction by gas effectively decays the orbit and then the GW drives the merger. The type A is seen in the cases with higher gas density and lower BH density, as expected. The examples of type A are shown in the top panels of Figs 1–4. In both types B and C, the strong disturbance of the orbit is induced by the three-body interaction during the first merger. But in type B, after the first few mergers by three-body interaction,

the orbit decays slowly for long time through the gas dynamical friction. The examples of type B are seen in the middle panels of Figs 2, 4, and 5. In these results, after the mergers driven by three-body interaction, the orbit evolution starts from a larger separation than initial typical separation ( $r_{\text{typ}}$ ). Such increase of separation is due to the slingshot mechanism when an intruder interacts with the binary. This causes a negative effect on the merger time-scale. In other words, the three-body interaction may play a positive and negative role for the merger.<sup>1</sup> In type C, the strong disturbance of the orbit continues until the final merger. The three-body interaction of BHs solely transfers the angular momentum, eventually allowing the merger via the GW radiation. Type C is seen in the cases of high BH density. The examples of type C are shown in the bottom panels of Figs 2 and 4.

As shown in Tables 1 and 2, in the cases of lower BH density (higher  $r_{\text{typ}}$ ), type A is seen in a broad range of gas density. In the

<sup>1</sup> In the present study, we assume the uniform gas. However, in a real galaxy, the gas distribution is likely to become diffuse in outer regions. If the velocity of the kicked BH is high enough, the BH cannot fall back but may escape.

**Table 2.** The results with  $M_{\text{BH}} = 10^4 M_{\odot}$  and  $N_{\text{BH}} = 10$ .

$r_{\text{typ}}$ (pc)	10.0		4.64		2.15		1.0		0.464		0.215		0.1	
	$\rho_{\text{BH}} (M_{\odot} \text{pc}^{-3})$	$N_{\text{m}}$ Type	$N_{\text{m}}$ Type											
$n_{\text{gas}} (\text{cm}^{-3})$	$t_{\text{fin}}$ (yr)		$t_{\text{fin}}$ (yr)		$t_{\text{fin}}$ (yr)		$t_{\text{fin}}$ (yr)		$t_{\text{fin}}$ (yr)		$t_{\text{fin}}$ (yr)		$t_{\text{fin}}$ (yr)	
10 <sup>12</sup>	0	–	4	A	7	A	9	A	9	A	9	A	9	A
	1.0 × 10 <sup>8</sup>		1.0 × 10 <sup>8</sup>		1.0 × 10 <sup>8</sup>		1.3 × 10 <sup>7</sup>		1.5 × 10 <sup>6</sup>		1.7 × 10 <sup>5</sup>		2.2 × 10 <sup>4</sup>	
10 <sup>11</sup>	0	–	5	A	9	A	9	A	9	A	9	A	9	B
	1.0 × 10 <sup>8</sup>		1.0 × 10 <sup>8</sup>		4.6 × 10 <sup>7</sup>		5.0 × 10 <sup>6</sup>		5.8 × 10 <sup>5</sup>		7.2 × 10 <sup>4</sup>		1.6 × 10 <sup>4</sup>	
10 <sup>10</sup>	4	A	8	A	9	A	9	A	9	A	9	A	9	B
	1.0 × 10 <sup>8</sup>		1.0 × 10 <sup>8</sup>		1.7 × 10 <sup>7</sup>		2.0 × 10 <sup>6</sup>		2.5 × 10 <sup>5</sup>		9.3 × 10 <sup>4</sup>		4.1 × 10 <sup>4</sup>	
10 <sup>9</sup>	5	A	9	A	9	A	9	A	9	B	9	B	9	B
	1.0 × 10 <sup>8</sup>		5.8 × 10 <sup>7</sup>		7.0 × 10 <sup>6</sup>		9.6 × 10 <sup>5</sup>		7.6 × 10 <sup>5</sup>		9.0 × 10 <sup>5</sup>		2.4 × 10 <sup>6</sup>	
5 × 10 <sup>8</sup>	5	A	9	A	9	A	9	B	9	B	9	B	9	B
	1.0 × 10 <sup>8</sup>		5.0 × 10 <sup>7</sup>		1.0 × 10 <sup>7</sup>		1.5 × 10 <sup>6</sup>		9.5 × 10 <sup>5</sup>		7.6 × 10 <sup>5</sup>		6.7 × 10 <sup>5</sup>	
10 <sup>8</sup>	7	A	9	A	9	B	9	B	9	B	9	B	9	B
	1.0 × 10 <sup>8</sup>		2.5 × 10 <sup>7</sup>		3.7 × 10 <sup>6</sup>		8.3 × 10 <sup>6</sup>		4.9 × 10 <sup>6</sup>		5.6 × 10 <sup>6</sup>		7.9 × 10 <sup>6</sup>	
5 × 10 <sup>7</sup>	9	A	9	A	9	B	9	B	9	B	9	B	9	B
	7.3 × 10 <sup>7</sup>		2.0 × 10 <sup>7</sup>		1.3 × 10 <sup>7</sup>		7.1 × 10 <sup>6</sup>		1.2 × 10 <sup>7</sup>		3.5 × 10 <sup>6</sup>		9.4 × 10 <sup>6</sup>	
10 <sup>7</sup>	9	B	9	B	9	B	9	B	9	B	9	B	9	B
	7.7 × 10 <sup>7</sup>		3.5 × 10 <sup>7</sup>		9.3 × 10 <sup>7</sup>		6.0 × 10 <sup>7</sup>		3.3 × 10 <sup>7</sup>		3.6 × 10 <sup>7</sup>		4.1 × 10 <sup>7</sup>	
5 × 10 <sup>6</sup>	8	B	9	B	9	B	9	B	9	B	9	B	9	B
	1.0 × 10 <sup>8</sup>		8.3 × 10 <sup>7</sup>		3.9 × 10 <sup>7</sup>		8.5 × 10 <sup>7</sup>		4.6 × 10 <sup>7</sup>		4.8 × 10 <sup>7</sup>		7.9 × 10 <sup>7</sup>	
10 <sup>6</sup>	5	B	7	B	4	B	9	B	5	C	5	C	6	C
	1.0 × 10 <sup>8</sup>		1.0 × 10 <sup>8</sup>		1.0 × 10 <sup>8</sup>		6.5 × 10 <sup>7</sup>		1.0 × 10 <sup>8</sup>		1.0 × 10 <sup>8</sup>		1.0 × 10 <sup>8</sup>	
5 × 10 <sup>5</sup>	3	B	3	C	3	C	3	C	6	C	4	C	4	C
	1.0 × 10 <sup>8</sup>		1.0 × 10 <sup>8</sup>		1.0 × 10 <sup>8</sup>		1.0 × 10 <sup>8</sup>		1.0 × 10 <sup>8</sup>		1.0 × 10 <sup>8</sup>		1.0 × 10 <sup>8</sup>	
10 <sup>5</sup>	0	–	0	–	0	–	0	–	0	–	1	C	0	–
	1.0 × 10 <sup>8</sup>		1.0 × 10 <sup>8</sup>		1.0 × 10 <sup>8</sup>		1.0 × 10 <sup>8</sup>		1.0 × 10 <sup>8</sup>		1.0 × 10 <sup>8</sup>		1.0 × 10 <sup>8</sup>	
5 × 10 <sup>4</sup>	0	–	0	–	1	C	0	–	1	C	1	C	1	C
	1.0 × 10 <sup>8</sup>		1.0 × 10 <sup>8</sup>		1.0 × 10 <sup>8</sup>		1.0 × 10 <sup>8</sup>		1.0 × 10 <sup>8</sup>		1.0 × 10 <sup>8</sup>		1.0 × 10 <sup>8</sup>	
10 <sup>4</sup>	0	–	0	–	0	–	0	–	0	–	0	–	1	C
	1.0 × 10 <sup>8</sup>		1.0 × 10 <sup>8</sup>		1.0 × 10 <sup>8</sup>		1.0 × 10 <sup>8</sup>		1.0 × 10 <sup>8</sup>		1.0 × 10 <sup>8</sup>		1.0 × 10 <sup>8</sup>	

cases of higher BH density, type B is dominant in higher gas density environments. On the other hand, type C is common in lower gas density. However, if the gas density is very low, no merger occurs even in the same density of BHs. This implies that the gas dynamical friction plays a non-negligible role even for type C.

### 3.3 BH number dependence

To clarify the physics of BH merger, we perform reference simulations with the different number of BHs. In Fig. 6, we compare the resultant merger time in 10 BH systems ( $t_{N=10}$ ) to that in three BH ( $t_{N=3}$ ) or two BH systems ( $t_{N=2}$ ). Each panel corresponds to a different set of parameters. Red, pink, and blue open symbols, respectively, represent the types A, B, and C mergers in 10 BH systems. Brown- and green-filled symbols show the averaged merger time in the runs of three BH and two BH systems, respectively. Note that the averaged merger time ( $t_{\text{fin}}$ ) has the variance of about a factor of 2 that comes from the initial set-up of random number.

In the cases of two BHs, we give only circular velocity initially. Since there is no three-body interaction, the merger of two BH systems is always driven by the gas dynamical friction. On the

other hand, in the systems of three BHs, three-body interaction as well as the gas dynamical friction can work to induce the merger. We can see that the merger time-scales in type C accord with those in three BH systems. In other words, no merger occurs in two BH systems in the parameters of type C. Thus, the classification of type C in which the merger is driven by the three-body interaction is justified.

On the other hand, in type A and type B, both two BH and three BH systems can merge. In the parameters of type A, the merger time-scales in 10 BH systems are systematically shorter than those in three BH systems. In the 10 BH systems, more BHs suffer from the gas dynamical friction and the angular momenta of BHs are extracted simultaneously. Therefore, the 10 BH systems can merge in shorter time on average. As shown in top left- and top right-hand panels, two BH or three BH systems cannot merge in higher gas density environments, whereas 10 BH systems can merge. These results imply that the dynamical friction on 10 BHs enhances the three-body interaction, eventually allowing the merger. In the bottom right-hand panel, the averaged merger time in 10 BH systems is slightly longer than that in three BH systems, in the cases with lower gas density ( $n_{\text{gas}} < 10^8 \text{ cm}^{-3}$ ). This is expected by the negative feedback as discussed in Section 3.2.

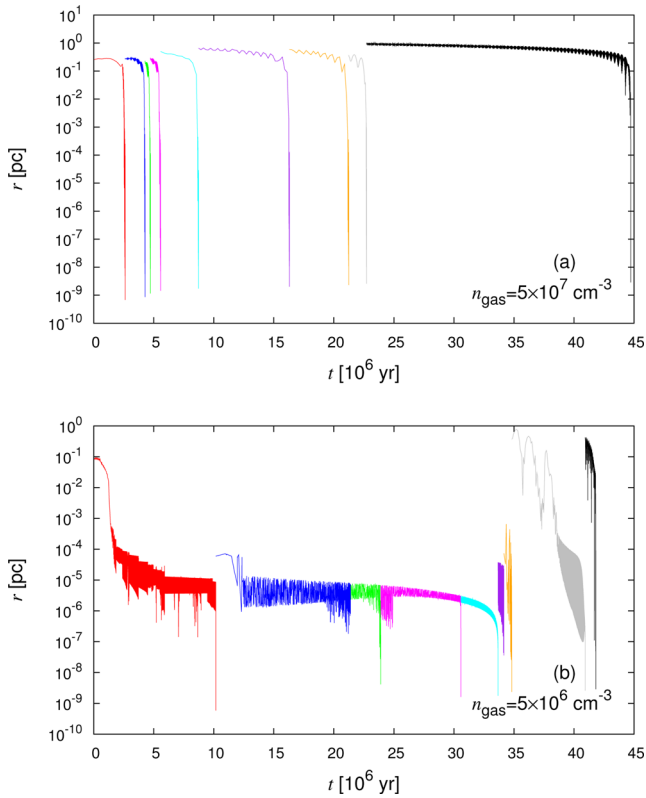


**Figure 1.** The separation of the closest pair within all BHs as a function of time. The initial BH mass is  $M_{\text{BH}} = 30 M_{\odot}$ , the initial typical extension of the BH distribution is  $r_{\text{typ}} = 1.0 \text{ pc}$ , and the gas density is  $n_{\text{gas}} = 5 \times 10^7 \text{ cm}^{-3}$  (top) or  $5 \times 10^6 \text{ cm}^{-3}$  (bottom).

### 3.4 Effect of recoil

In the above, we have not considered the effects of GW recoil. The recoil velocity ranges from several tens to several thousands  $\text{km s}^{-1}$  (Kesden, Sperhake & Berti 2010). Tanikawa & Umemura (2014) have shown that if the recoil velocity is lower than the virial velocity in the system, multiple BHs can eventually merge. In the present simulations, the virial velocity is higher than a few hundreds  $\text{km s}^{-1}$  for  $n_{\text{gas}} \geq 10^8 \text{ cm}^{-3}$  and  $M_{\text{gas}} \geq 10^6 M_{\odot}$  in the case of  $M_{\text{BH}} = 30 M_{\odot}$ , and for  $n_{\text{gas}} \geq 10^6 \text{ cm}^{-3}$  and  $M_{\text{gas}} \geq 10^7 M_{\odot}$  in the case of  $M_{\text{BH}} = 10^4 M_{\odot}$ . Actually, we have imposed random velocities on BHs at a level of the virial velocity, and revealed the conditions under which all BHs can merge. Hence, the merger condition is expected not to change, if the recoil velocity is lower than the virial velocity. To confirm this, we have simulated the several cases in which the recoil velocity is incorporated. As a result, we have found that if the recoil velocity is lower than the virial (escape) velocity, then the averaged merger time and the number of merged BHs are not changed. If the recoil velocity is higher than the escape velocity, then the merged BH escapes from the system. The actual magnitude of recoil velocity is determined by the alignment of spins of two MBHs (Schnittman & Buonanno 2007; Kesden et al. 2010). The spins tend to be aligned through the gas accretion on to BHs. Assuming the level of the recoil velocity for BHs with aligned spins, we have performed further simulations and found that if the escape velocity of the system is higher than  $\sim 140 \text{ km s}^{-1}$ , then the BH merger proceeds in a similar way to the simulations without the recoil.

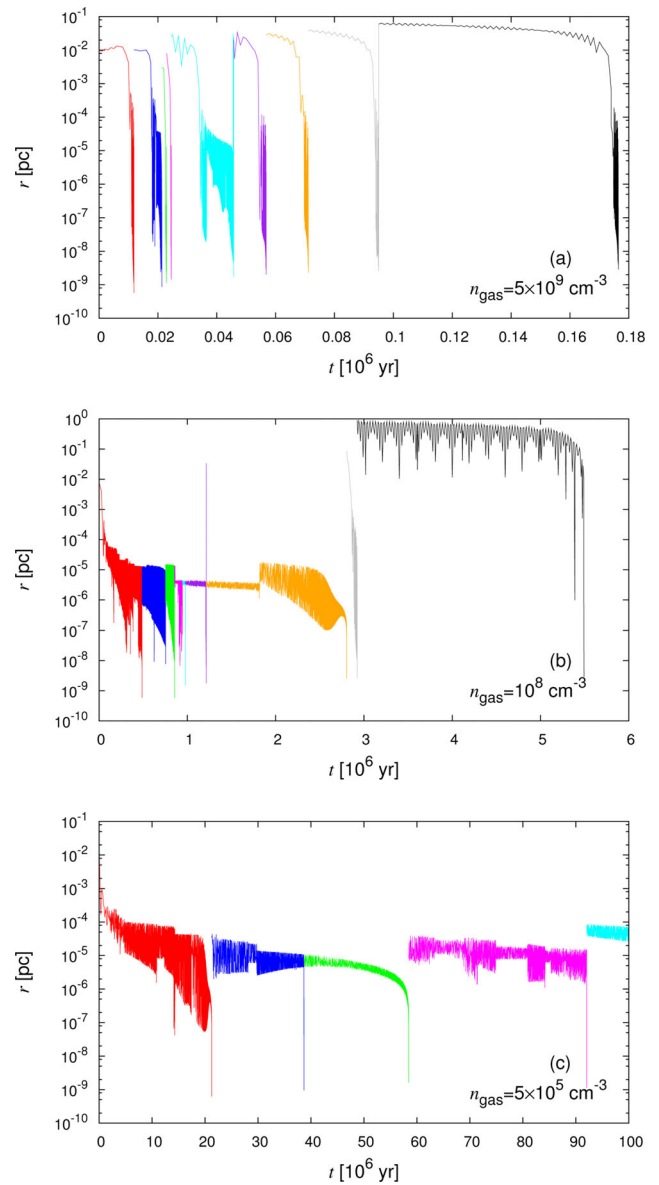


**Figure 2.** Same as Fig. 1, but for  $r_{\text{typ}} = 0.1 \text{ pc}$ , and  $n_{\text{gas}} = 5 \times 10^9$  (top),  $10^8$  (middle), or  $5 \times 10^5 \text{ cm}^{-3}$  (bottom).

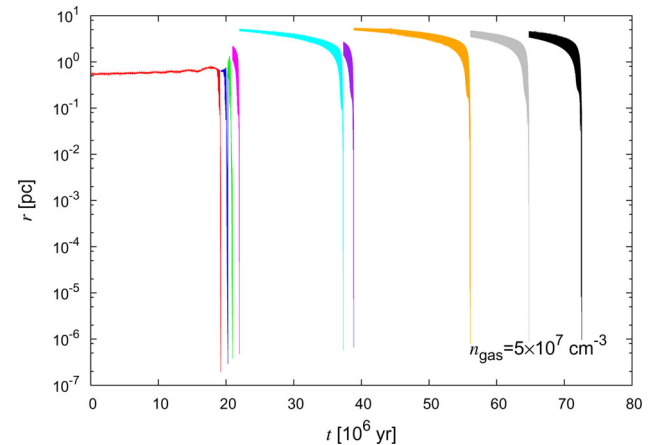


**Figure 3.** Same as Fig. 1, but for  $M_{\text{BH}} = 10^4 M_{\odot}$ ,  $r_{\text{typ}} = 10.0 \text{ pc}$ , and  $n_{\text{gas}} = 5 \times 10^7 \text{ cm}^{-3}$ .

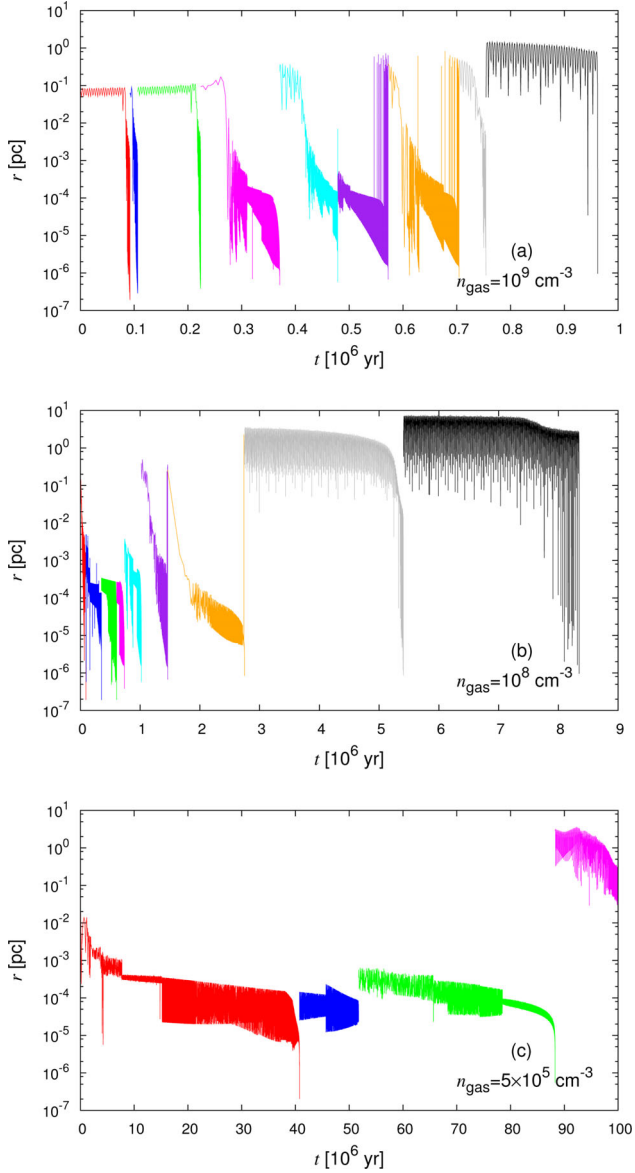


**Figure 4.** Same as Fig. 1, but for  $M_{\text{BH}} = 10^4 M_{\odot}$ ,  $r_{\text{typ}} = 1.0$  pc, and  $n_{\text{gas}} = 10^9$  (top),  $10^8$  (middle), or  $5 \times 10^5 \text{ cm}^{-3}$  (bottom).

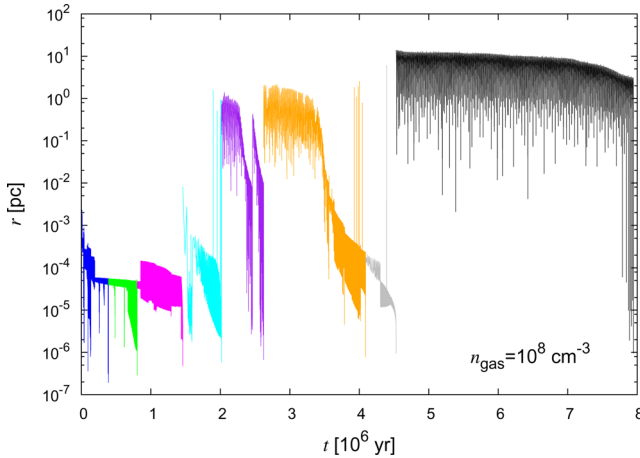


**Figure 5.** Same as Fig. 1, but for  $M_{\text{BH}} = 10^4 M_{\odot}$ ,  $r_{\text{typ}} = 0.1$  pc, and  $n_{\text{gas}} = 10^8 \text{ cm}^{-3}$ .

#### 4 CRITERION FOR GAS DRAG

In Fig. 7, we compare the averaged merger time in 10 BH systems ( $t_{N=10}$ ) to the analytic estimate of gas dynamical friction time-scale ( $t_{\text{DF}}$ ). We assess the friction time-scale assuming a binary BH, similar to those by Begelman et al. (1980) and Matsubayashi, Makino & Ebisuzaki (2007). Based on a test simulation for a BH binary, we postulate that the eccentricity of the binary becomes very high, when the BH gravity dominates the gas potential. Then,  $t_{\text{DF}}$  is estimated as

$$t_{\text{DF}} = \int_{100 r_{\text{sch}}}^{r_{\text{typ}}} \frac{\tilde{t}_{\text{DF}}(r)}{r} dr, \quad (19)$$

$$\tilde{t}_{\text{DF}}(r) \equiv \frac{v_{\text{circ}}(r)}{\max\{a_{\text{DF}}^{\text{gas}}(r')\}} \cdots r \leq r' \leq r_{\text{typ}}, \quad (20)$$

$$\tilde{t}_{\text{DF}}(r_{\text{typ}}) \simeq \frac{v_{\text{circ}}^3}{4\pi G^2 M_{\text{BH}} m_{\text{H}} n_{\text{gas}}} \quad (21)$$

$$\simeq \begin{cases} \frac{(4\pi m_{\text{H}} n_{\text{gas}})^{1/2} r_{\text{typ}}^3}{3^{3/2} G^{1/2} M_{\text{BH}}} (M_{\text{gas,b}} \gg M_{\text{BH}}), \\ \frac{M_{\text{BH}}^{1/2}}{4\pi G^{1/2} m_{\text{H}} n_{\text{gas}} r_{\text{typ}}^{3/2}} (M_{\text{gas,b}} \ll M_{\text{BH}}). \end{cases} \quad (22)$$

Here,  $M_{\text{gas,b}}$  is the gas mass within the binary orbit, and  $v_{\text{circ}}$  is the circular velocity given as  $v_{\text{circ}} = [G(2M_{\text{gas,b}} + M_{\text{BH}})/2r]^{1/2}$ . In this estimate, we use the maximum value of  $a_{\text{DF}}^{\text{gas}}$  in the range of  $r \leq r' \leq r_{\text{typ}}$ . Green curves in Fig. 7 present the estimated time-scale of gas dynamical friction. According to equation (22),  $t_{\text{DF}}$  is proportional to  $n_{\text{gas}}^{1/2}$  in the limit of high gas density, whereas  $t_{\text{DF}}$  is inversely proportional to  $n_{\text{gas}}$  in the limit of low gas density. Thus, a turning point (the minimum) emerges in each curve of  $t_{\text{DF}}$  due to this change of dependence. As seen in Fig. 7, the turning point is in accordance with the transition from type A (gas-drag-driven merger) to type B (interplay-driven merger), and also the trend of merger time ( $t_{N=10}$ ) is in agreement with the analytic estimate of gas dynamical friction time-scale ( $t_{\text{DF}}$ ). The time-scale becomes longer in the higher gas density due to the increase in the deepness of gravitational potential of gas. The longer time-scale in the lower gas density stems from the strong gravitational potential of other BHs. In addition, we can recognize the difference that the analytic estimate is systematically longer than the merger time in the simulations. One reason for the systematic difference comes from dismissing the GW as well as the three-body interaction effect in the analytic estimate. Another reason is concerns the fact that the analytic time-scale is based on the approximate values of initial positions in type B and type C.

In Fig. 7, we see the dependence of the merger time-scale on the BH density (or  $r_{\text{typ}}$ ). With the increasing BH density (decreasing  $r_{\text{typ}}$ ), the right-hand side of the power-law shifts lower. This shift stems from the decrease in the gravitational potential of gas within  $r_{\text{typ}}$ . This tendency is also seen in the numerical results of 10 BH systems. Thus, the rough tendency of the merger time in the type A region is explained by the analytic time-scale. Therefore, we regard  $t_{\text{DF}}$  as an appropriate estimate for the merger solely by the gas dynamical friction.

As described above, type A is always seen in higher gas density than the turning point of the double power law of  $t_{\text{DF}}$ . These results imply that the turning point provides the critical gas density, above which the merger is driven by the gas dynamical friction. The turning point is determined by the ratio of the gas mass within  $r_{\text{typ}}$ ,  $M_{\text{gas}}$ , to the total BH mass,  $\sum M_{\text{BH}}$ . In the analytic estimate, the turning

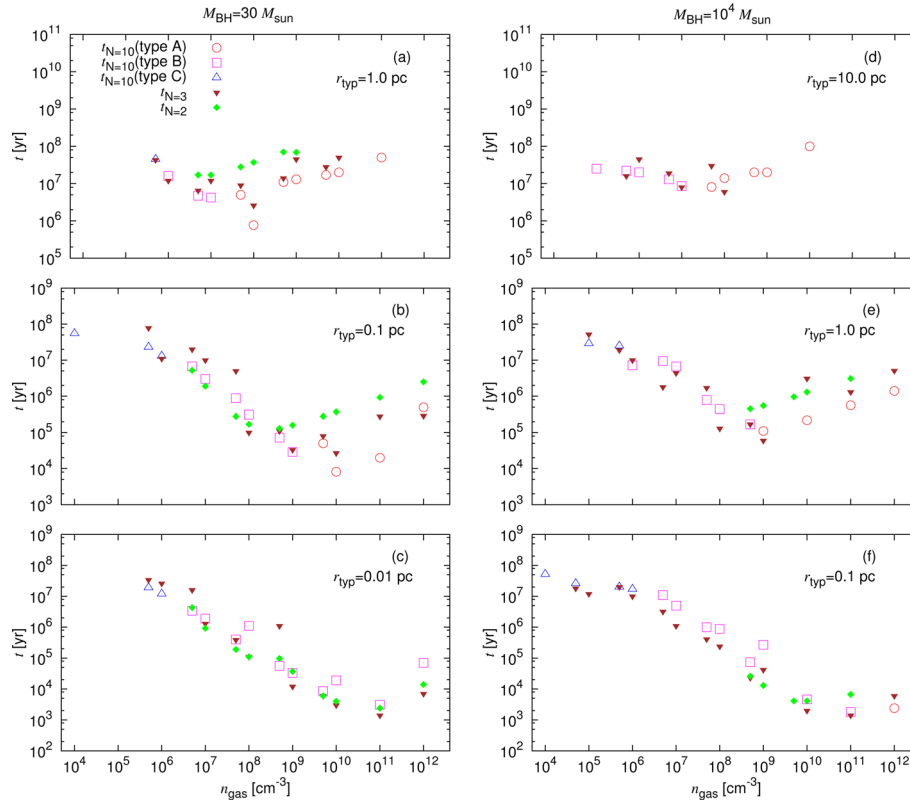


**Figure 6.** Merger time in 10 BH systems ( $t_{N=10}$ ) as a function of gas number density  $n_{\text{gas}}$ . The left-hand panels are the cases with low-mass BHs ( $M_{\text{BH}} = 30 M_{\odot}$ ), and right-hand panels are those with high-mass BHs ( $M_{\text{BH}} = 10^4 M_{\odot}$ ). The top, middle, and bottom panels show the results for lower, intermediate, and higher BH density, respectively. Red, pink, and blue open symbols represent the results of the types A, B, and C mergers, respectively. Green- and brown-filled symbols are the results of two BH ( $t_{N=2}$ ) and three BH ( $t_{N=3}$ ) systems, respectively.

point appears around  $M_{\text{gas}} \simeq 1.4 \times 10^5 \sum M_{\text{BH}}$  as the average of the each panel in Fig. 7. As for the numerical results, we can assess the turning points in the top and middle panels, since the turning points are not clear in the bottom panels. In the cases of  $30 M_{\odot}$  BHs, the gas density at the turning points is  $10^7 \text{ cm}^{-3}$  in upper left-hand panel or  $10^{10} \text{ cm}^{-3}$  in middle left-hand panels. Then, the ratio of  $M_{\text{gas}}$  to  $\sum M_{\text{BH}}$  at the turning points is  $1.4 \times 10^5$  in both cases. In the cases of  $10^4 M_{\odot}$  BHs, it is  $10^7 \text{ cm}^{-3}$  in upper right-hand panel, or  $10^9 \text{ cm}^{-3}$  in middle right-hand panels. Hence, the  $M_{\text{gas}}$ -to- $\sum M_{\text{BH}}$  ratio is  $4.2 \times 10^5$  or  $4.2 \times 10^4$ , respectively. These results show that the critical gas density above which type A is dominant is given by the condition of  $M_{\text{gas}}/\sum M_{\text{BH}} \approx 10^5$ . Based on the simulations on the formation of first objects (Greif et al. 2011; Susa et al. 2014),  $M_{\text{gas}}$  is likely to be lower than  $10^5 \sum M_{\text{BH}}$ . Thus, type B and type C are expected to be more common mechanism of BH merger.

## 5 CONCLUSIONS

In this paper, we have investigated the merger of multiple BH systems in an early cosmic epoch, incorporating the dynamical friction by gas. For the purpose, we have performed highly accurate numerical simulations taking into account such general relativistic effects as the pericentre shift and GW emission. Consequently, we have found the following.

(1) Multiple BHs are able to merge into one BH within 100 Myr in a wide range of parameters. In the case of  $M_{\text{BH}} = 30 M_{\odot}$ , if  $n_{\text{gas}}$  is in the range from  $5 \times 10^6$  to  $10^8 \text{ cm}^{-3}$ , then all the BHs can merge for the BH density of  $\rho_{\text{BH}} = 72\text{--}7.2 \times 10^7 M_{\odot} \text{ pc}^{-3}$ . In the case of

$M_{\text{BH}} = 10^4 M_{\odot}$ , if  $n_{\text{gas}}$  is in the range from  $5 \times 10^6$  to  $10^9 \text{ cm}^{-3}$ , then all the BHs can merge for the BH density of  $\rho_{\text{BH}} = 2.4 \times 10^2\text{--}2.4 \times 10^7 M_{\odot} \text{ pc}^{-3}$ . Commonly, if the gas density is higher than  $n_{\text{gas}} = 5 \times 10^5 \text{ cm}^{-3}$ , the BH merger occurs once at least in 100 Myr.

(2) The merger mechanism is classified into three types: gas-drag-driven merger (type A), three-body-driven merger (type C), and interplay-driven merger (type B). A criterion between type B and type C is almost concordant with the results of two BH or three BH systems.

(3) Based on the argument of merger time-scales, type A merger has turned out to occur, if the gas mass within the initial BH orbit ( $M_{\text{gas}}$ ) is higher than  $10^3 \sum M_{\text{BH}}$ , where  $\sum M_{\text{BH}}$  is the total mass of BHs.

(4) Supposing the gas and BH density based on the recent numerical simulations on first stars (Greif et al. 2011; Umemura et al. 2012, Susa 2013; Susa et al. 2014), all the BH remnants from first stars are likely to merge into one BH in  $\sim 10^7$  yr through the type B or C mechanism.

(5) As for a primordial galaxy possessing MBHs with  $M_{\text{BH}} = 10^4 M_{\odot}$ , it is suggested that in environments of gas density higher than  $5 \times 10^6 \text{ cm}^{-3}$ , multiple BHs can merge into one through the type B mechanism, even if the typical separation is greater than several pc. This result implies that the BH merger is able to contribute significantly to the formation of SMBHs at high redshifts.

A point we have not considered in this paper is the effect of mass accretion on to BHs. During the motion of BHs in gas, some gas can fall on to BHs through the Bondi–Hoyle–Littleton accretion. This

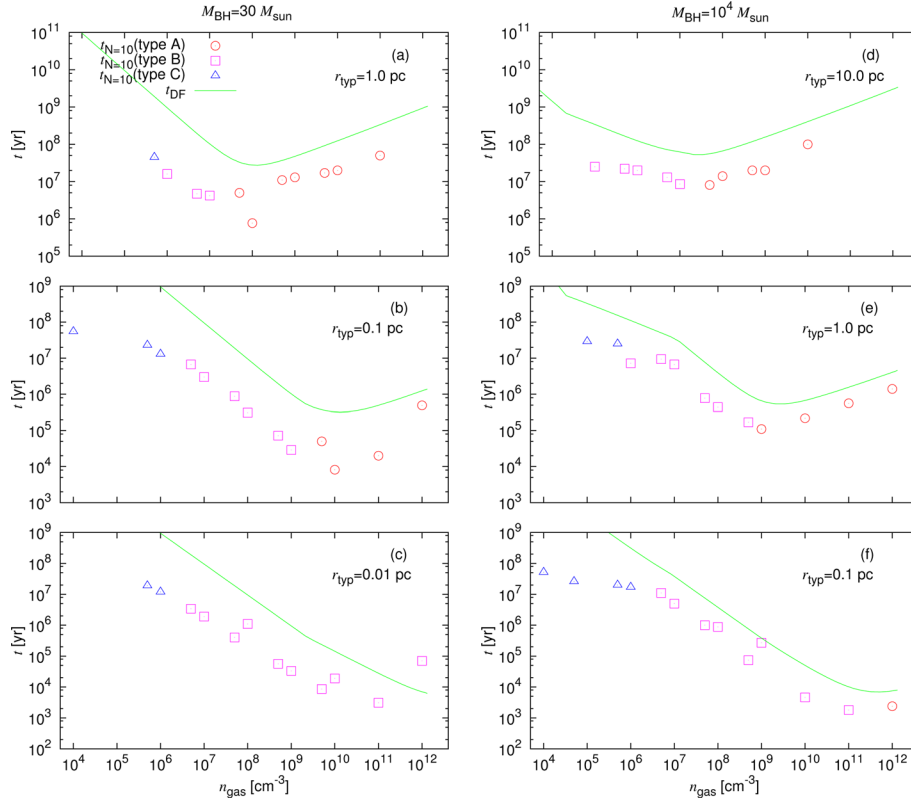


**Figure 7.** Same as Fig. 6, but the analytic estimates of gas dynamical friction time-scale,  $t_{DF}$ , are plotted by green lines instead of the results of two BH and three BH systems.

effect may significantly affect the merger processes of BHs. This issue will be studied in a forthcoming paper. Besides, in a primordial galaxy, the stellar dynamical friction may work cooperatively with the gas friction to extract the angular momenta. Such synergism is also an issue to be explored in the future.

## ACKNOWLEDGEMENTS

Numerical computations and analyses were carried out on Cray XC30 and computers at Center for Computational Astrophysics, National Astronomical Observatory of Japan, respectively. This work was supported in part by Grant-in-Aid for Scientific Research (B) by JSPS (15H03638).

## REFERENCES

- Abel T., Bryan G. L., Norman M. L., 2000, *ApJ*, 540, 39  
 Alvarez M. A., Wise J. H., Abel T., 2009, *ApJ*, 701, L133  
 Begelman M. C., Blandford R. D., Rees M. J., 1980, *Nature*, 287, 307  
 Bromm V., Loeb A., 2003, *ApJ*, 596, 34  
 Bromm V., Coppi P. S., Larson R. B., 2002, *ApJ*, 564, 23  
 Escala A., Larson R. B., Coppi P. S., Mardones D., 2004, *ApJ*, 607, 765  
 Escala A., Larson R. B., Coppi P. S., Mardones D., 2005, *ApJ*, 630, 152  
 Fan X. et al., 2001, *AJ*, 122, 2833  
 Greene J. E., 2012, *Nat. Commun.*, 3, 1304  
 Greif T. H., Springel V., White S. D. M., Glover S. C. O., Clark P. C., Smith R. J., Klessen R. S., Bromm V., 2011, *ApJ*, 737, 75  
 Haiman Z., 2013, in Wiklund T., Moberg B., Bromm V., eds, *Astrophysics and Space Science Library*, Vol. 396, *The First Galaxies*. Springer-Verlag, Berlin, p. 293  
 Heger A., Woosley S. E., 2002, *ApJ*, 567, 532  
 Hirano S., Hosokawa T., Yoshida N., Umeda H., Omukai K., Chiaki G., Yorke H. W., 2014, *ApJ*, 781, 60  
 Hollenbach D., McKee C. F., 1989, *ApJ*, 342, 306  
 Inayoshi K., Omukai K., 2012, *MNRAS*, 422, 2539  
 Iwasawa M., Funato Y., Makino J., 2006, *ApJ*, 651, 1059  
 Kesden M., Sperhake U., Berti E., 2010, *ApJ*, 715, 1006  
 Khan F. M., Just A., Merritt D., 2011, *ApJ*, 732, 89  
 Khan F. M., Preto M., Berczik P., Berentzen I., Just A., Spurzem R., 2012, *ApJ*, 749, 147  
 Khan F. M., Holley-Bockelmann K., Berczik P., Just A., 2013, *ApJ*, 773, 100  
 Kim W.-T., El-Zant A., Kamionkowski M., 2005, *ApJ*, 632, 157  
 Kormendy J., Ho L. C., 2013, *ARA&A*, 51, 511  
 Kupi G., Amaro-Seoane P., Spurzem R., 2006, *MNRAS*, 371, 45  
 Kurk J. D. et al., 2007, *ApJ*, 669, 32  
 Makino J., Aarseth S., 1992, *PASJ*, 44, 141  
 Matsubayashi T., Makino J., Ebisuzaki T., 2007, *ApJ*, 656, 879  
 Merritt D., Poon M. Y., 2004, *ApJ*, 606, 788  
 Milosavljevic M., Couch S. M., Bromm V., 2009, *ApJ*, 696, 146  
 Mortlock D. J. et al., 2011, *Nature*, 474, 616  
 Nakamura F., Umemura M., 2001, *ApJ*, 548, 19  
 Omukai K., 2000, *ApJ*, 534, 809  
 Ostriker E. C., 1999, *ApJ*, 513, 252  
 Palla F., Salpeter E. E., Stahler S. W., 1983, *ApJ*, 271, 632  
 Schnittman J. D., Buonanno A., 2007, *ApJ*, 662, 63  
 Susa H., 2013, *ApJ*, 773, 185  
 Susa H., Umemura M., 2004, *ApJ*, 600, 1  
 Susa H., Hasegawa K., Tominaga N., 2014, *ApJ*, 792, 32  
 Tanaka T., Haiman Z., 2009, *ApJ*, 696, 1798  
 Tanikawa A., Umemura M., 2011, *ApJ*, 728, L31  
 Tanikawa A., Umemura M., 2014, *MNRAS*, 440, 652

Thoul A. A., Weinberg D. H., 1995, ApJ, 442, 480  
Umemura M., Loeb A., Turner E. L., 1993, ApJ, 419, 459  
Umemura M., Susa H., Hasegawa K., Suwa T., Semelin B., 2012, Progress  
Theor. Exp. Phys., 2012, 01A306  
Vasiliev E., Antonini F., Merritt D., 2014, ApJ, 785, 163  
Volonteri M., Bellovary J., 2012, Rep. Progress Phys., 75, 124901

Wu X.-B. et al., 2015, Nature, 518, 512  
Yoshida N., Omukai k., Hernquist L., Abel T., 2006, ApJ, 652, 6

This paper has been typeset from a  $\text{\TeX}/\text{\LaTeX}$  file prepared by the author.